Effective isoscalar nucleon-nucleon interactions at 500 MeV

M. L. Barlett, W. R. Coker, G. W. Hoffmann, and L. Ray
Department of Physics, The University of Texas at Austin, Austin, Texas 78712
(Received 20 October 1983)

The 500 MeV effective nucleon-nucleon isoscalar interaction is investigated through nonrelativistic folding model analyses of $\vec{p}$ + nucleus elastic scattering data. Three empirical interactions are deduced. The first, obtained from a relativistic-Schrödinger-equation-equivalent form of a phenomenological Dirac optical potential, contains terms which are dependent on the square of the nuclear matter density. A modified version of this interaction is then obtained, in which the density dependence is made explicit. Finally, an optical potential is deduced which depends linearly on the density, resulting in a density-independent nucleon-nucleon effective interaction. Nuclear size information inferred from calculations using these effective interactions is found to be in reasonable agreement with theoretical expectations. The relative merits of each of these three forms of the interaction are discussed.

I. INTRODUCTION

Use of the impulse approximation (IA) to generate nonrelativistic multiple scattering optical potentials, such as defined by Kerman, McManus, and Thaler (KMT),[1] does not always lead to adequate descriptions of 500 and 800 MeV proton + nucleus (pA) elastic scattering observables.[2,3] Theoretical investigations[2,4–6] at these energies suggest that omission of nuclear medium modifications (e.g., Pauli blocking and binding effects in intermediate scattering states) and/or relativistic effects may be responsible for many of the shortcomings.

In the past, analyses of pA elastic scattering in terms of microscopic optical potentials have emphasized obtaining reliable information regarding the relative differences between the neutron density distributions of neighboring isotopes.[7] However, such work has provided little or no insight into what the *effective* nucleon-nucleon (NN) interaction in nuclei may be like.

In the present work, we have reversed the usual procedures. We assume that the nuclear matter densities are well determined, and use the 500 MeV pA elastic scattering observables[2,8,9] to deduce the effective interaction at this energy. We use a conventional folding model for the nonrelativistic nucleon-nucleus optical potential. The deduced amplitudes are suitable for direct use in most existing computer programs for analysis of medium energy scattering data.

Three sets of effective isoscalar interactions are obtained. The first is unfolded from the successful Dirac equation optical potential phenomenology.[10] The second is an alternate density-dependent version of the first, while the third is of the standard KMT-type "$t\rho$" form. The best overall description of the 500 MeV pA elastic scattering data is provided by the first interaction model, the latter two being accurate at forward angles only. In each case local, spin-dependent pA optical potentials are generated. It is intended that these interactions will be applicable in other types of proton-nucleus reaction calculations at and near 500 MeV and that the results presented here will stimulate theoretical work which will provide an understanding of the effective amplitudes. The interaction models are discussed in Secs. II and III, while their limitations are pointed out in Sec. IV. A summary of results and the conclusions are given in Sec. V.

II. INTERACTION 1

A. Density-squared model

Phenomenological Dirac equation optical potentials of simple Woods-Saxon (densitylike) forms have led to good descriptions of much of the intermediate energy pA elastic scattering data.[10] Standard reduction techniques[10] enable us to obtain the upper (large) components of the four-component pA wave function from solution of an uncoupled, second order, Schrödinger-type differential equation. Elastic scattering observables constructed from these large components agree well with the observables computed using the full four-component Dirac wave function for 500 MeV pA scattering. Thus, we can construct a Schrödinger equivalent optical potential directly from the 500 MeV p + ^{40}Ca Dirac optical model. In terms of the scalar (U_s) and vector (U_v) Dirac optical potentials, the Schrödinger equivalent nuclear central potential[10] is

$$U^{c}_{\rm opt}(r)=\frac{1}{2E}\left[2EU_v+2mU_s-U_v^2+U_s^2-2U_vU_{\rm Coul}-\frac{(\hbar c)^2}{2r^2A(r)}\frac{\partial}{\partial r}\left[r^2\frac{\partial A}{\partial r}\right]+\frac{3}{4}\frac{(\hbar c)^2}{A(r)^2}\left[\frac{\partial A}{\partial r}\right]^2\right], \quad (1)$$

and the nuclear spin-orbit potential is

$$U^{\rm so}_{\rm opt}(r)=-\frac{(\hbar c)^2}{2EA(r)}\frac{1}{r}\frac{\partial A}{\partial r}. \quad (2)$$

In Eqs. (1) and (2), m is the proton mass, E is the proton total energy in the pA center-of-momentum (c.m.) system,

$U_{\rm Coul}$ is the Coulomb potential, and

$$A(r)=(E+m+U_s-U_v)/(E+m)\ .$$

The resulting local optical potential (almost purely isoscalar) in Eqs. (1) and (2) can then be cast in the form

$$U_{\rm opt}^{\rm isoscalar}(\vec{r})=\lambda\int_0^\infty q^2dq\,a(q)\widetilde{F}_c(q)j_0(qr)+\lambda\frac{i}{r}\frac{\partial}{\partial r}\left[\int_0^\infty q^2dq\,\tilde{c}(q)\widetilde{F}_{\rm so}(q)j_0(qr)\right]\vec{\sigma}\cdot\vec{1}\ , \tag{3}$$

where the isoscalar nucleon-nucleon effective interaction in the scattering amplitude form is defined by

$$f_{\rm NN}(q)=a(q)+c(q)\vec{\sigma}\cdot\hat{n}+\cdots\ ,$$

with

$$\tilde{c}(q)=\frac{c(q)}{k_{\rm N}^2\sin\theta_{\rm N}}\ ,$$

$$\theta_{\rm N}=2\sin^{-1}(q/2k_{\rm N})\ ,$$

and

$$\lambda=\frac{-4\pi(\hbar c)^2k_L\eta}{(2\pi)^2E_Lk_0}\ .$$

Here $a(q)$ and $c(q)$ are the complex proton-nucleon (pN) spin-independent and spin-orbit effective scattering amplitudes, $\widetilde{F}_{c,{\rm so}}(q)$ is a target dependent form factor, $k_{\rm N}$ is the relative momentum in the projectile-nucleus c.m. system, k_L is the momentum of the projectile in the laboratory system, E_L is the total energy of the projectile in the laboratory system, k_0 is the projectile momentum in the NN c.m. frame, and η is a kinematic factor which is defined in Ref. 1.

In order to determine $a(q)$ and $c(q)$ it is necessary to assume functional forms for the target form factors, $\widetilde{F}_{c,{\rm so}}(q)$. These are taken to be a function of the Fourier transform of the matter density, $\tilde{\rho}_m(q)$, since only the isoscalar part of the effective interaction is being studied. The matter density was generated by summing the ^{40}Ca proton and neutron point densities. The point proton density was obtained from the charge density,[11] while the neutron density was obtained from the prescription

$$\rho_{\rm n}(r)=\rho_{\rm p}(r)\,|_{(e,e')}+\rho_{\rm n}(r)\,|_{\rm HF}-\rho_{\rm p}(r)\,|_{\rm HF}\ , \tag{4}$$

where HF denotes a Hartree-Fock density[12] and $\rho_{\rm p}(r)\,|_{(e,e')}$ is the empirical proton density. During the fitting procedures, the matter densities were held fixed at the values obtained by the above-mentioned method. The

TABLE I. Interaction 1: Target form factor coefficients and effective isoscalar pN scattering amplitudes.

	Re(a)	Im(a)	Re(c)	Im(c)
z_i (fm^3)	−14.295	1.259	1.742	0.037
	Effective isoscalar scattering amplitudes (fm)			
q (fm^{-1})	Re(a)	Im(a)	Re(c)	Im(c)
0.000	0.4463×10^{-1}	0.5941	0.0	0.0
0.125	0.5237×10^{-1}	0.5904	0.1677×10^{-1}	0.3424×10^{-1}
0.250	0.7366×10^{-1}	0.5876	0.3342×10^{-1}	0.6679×10^{-1}
0.375	0.1015	0.5832	0.4979×10^{-1}	0.9615×10^{-1}
0.500	0.1286	0.5771	0.6579×10^{-1}	0.1212
0.625	0.1495	0.5697	0.8130×10^{-1}	0.1414
0.750	0.1617	0.5614	0.9627×10^{-1}	0.1567
0.875	0.1652	0.5526	0.1107	0.1679
1.000	0.1616	0.5440	0.1247	0.1760
1.125	0.1533	0.5362	0.1385	0.1825
1.250	0.1425	0.5268	0.1500	0.1867
1.375	0.1313	0.5116	0.1590	0.1890
1.500	0.1207	0.4952	0.1660	0.1880
1.625	0.1103	0.4728	0.1728	0.1855
1.750	0.9908×10^{-1}	0.4560	0.1780	0.1820
1.875	0.8757×10^{-1}	0.4289	0.1827	0.1783
2.000	0.7372×10^{-1}	0.4044	0.1860	0.1730
2.125	0.6105×10^{-1}	0.3891	0.1900	0.1680
2.250	0.5209×10^{-1}	0.3831	0.1922	0.1630
2.375	0.4416×10^{-1}	0.3836	0.1940	0.1580
2.500	0.3615×10^{-1}	0.3863	0.1940	0.1505

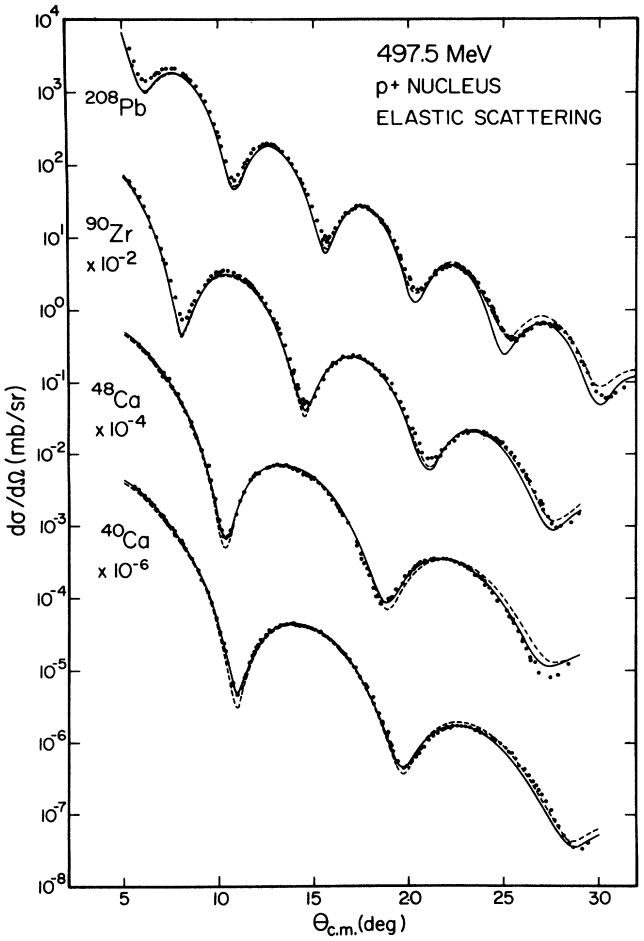

FIG. 1. Optical model predictions compared to differential cross section data (Ref. 2) for 500 MeV elastic scattering using interaction 1 (solid curves) and interaction 2 (dashed curves).

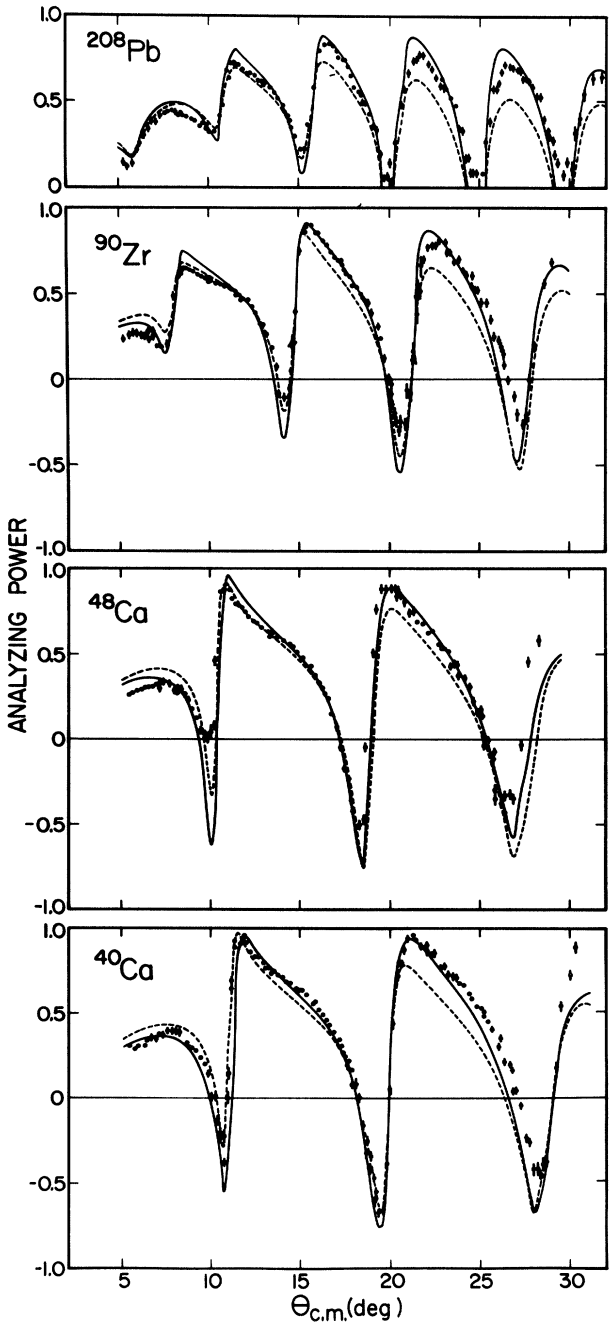

FIG. 2. Optical model predictions compared to 500 MeV elastic analyzing power data (Ref. 2) using interaction 1 (solid curves) and interaction 2 (dashed curves).

Schrödinger-equivalent optical potentials contain terms which depend linearly and quadratically on the Dirac scalar and vector potentials [see Eqs. (1) and (2)], which themselves have Woods-Saxon (densitylike) geometries. The quadratic (ρ^2) contributions represent intermediate scatterings of negative energy states of the projectile which have been projected out of the relativistic propagator in solving for the large components of the Dirac wave function and therefore appear in the Schrödinger-equivalent optical potential. Intermediate propagation of negative energy states of the projectile is an automatic feature of Dirac equation descriptions of scattering processes. Therefore, in order to develop a folding model which will successfully reproduce the Schrödinger equivalent of the Dirac pA optical potential, it is necessary to assume a more general form for the $\tilde{F}_{c,\mathrm{so}}(q)$ than $\tilde{F}_{c,\mathrm{so}} = \tilde{\rho}_m$. The form adopted here is

$$\tilde{F}_i(q) = \tilde{\rho}_m(q) + z_i \tilde{\rho}_m^2(q) , \tag{5}$$

where $\tilde{\rho}_m^2$ represents the Fourier transform of the square of the matter density. The coefficients, z_i, of the density-squared terms were fixed for each part of the optical potential (real, imaginary central and real, imaginary spin orbit) by demanding that the first zero of the Fourier-transformed Schrödinger-equivalent optical potential and the first zero of the target form factor occur at the same momentum transfer. The values of the coefficients, z_i, are given in Table I. The density squared term is mainly important for the real, central optical potential. The $a(q)$ and $c(q)$ were then adjusted in order to reproduce each

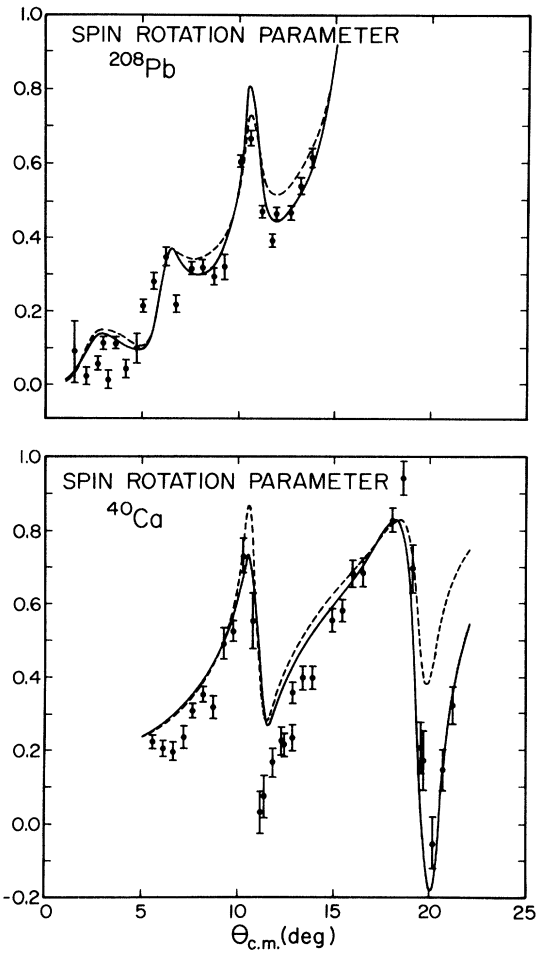

FIG. 3. Optical model predictions compared to 500 MeV elastic spin-rotation data (Refs. 8 and 9) using interaction 1 (solid curves) and interaction 2 (dashed curves).

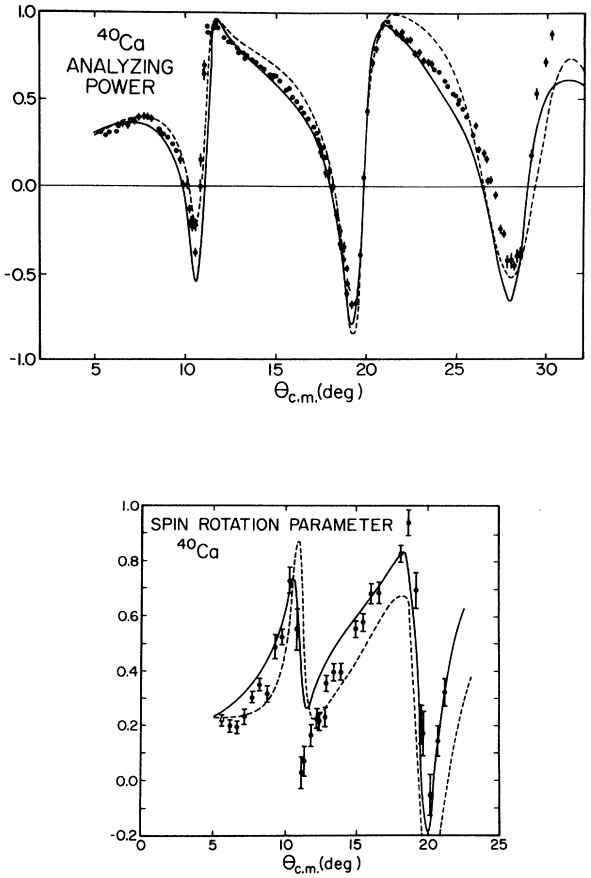

FIG. 4. Optical model predictions compared to 500 MeV $\vec{p}+{}^{40}$Ca elastic analyzing power (Ref. 2) and spin-rotation data (Ref. 8) using interaction 1 (solid curves) and interaction 1 reformulated to include explicit density dependence (dashed curves) as discussed in the text.

TABLE II. Interaction 2: Effective isoscalar pN scattering amplitudes in fm.

q (fm^{-1})	Re(a)	Im(a)	Re(c)	Im(c)
0.000	0.4085×10^{-1}	0.5806	0.0000	0.0000
0.125	0.3399×10^{-1}	0.5861	0.1792×10^{-1}	0.3449×10^{-1}
0.250	0.2081×10^{-1}	0.5884	0.3565×10^{-1}	0.6735×10^{-1}
0.375	0.2067×10^{-1}	0.5877	0.5306×10^{-1}	0.9722×10^{-1}
0.500	-0.2157×10^{-1}	0.5842	0.6998×10^{-1}	0.1231
0.625	-0.4910×10^{-1}	0.5782	0.8631×10^{-1}	0.1443
0.750	-0.7936×10^{-1}	0.5699	0.1020	0.1610
0.875	−0.1112	0.5600	0.1170	0.1739
1.000	−0.1434	0.5488	0.1314	0.1842
1.125	−0.1747	0.5367	0.1453	0.1930
1.250	−0.2042	0.5243	0.1584	0.2015
1.375	−0.2310	0.5118	0.1693	0.2076
1.500	−0.2544	0.4994	0.1793	0.2121
1.625	−0.2740	0.4874	0.1881	0.2134
1.750	−0.2896	0.4759	0.1950	0.2131
1.875	−0.3010	0.4647	0.2016	0.2099
2.000	−0.3085	0.4539	0.2073	0.2046
2.125	−0.3123	0.4433	0.2127	0.1969
2.250	−0.3125	0.4328	0.2172	0.1866
2.375	−0.3096	0.4219	0.2207	0.1779
2.500	−0.3039	0.4109	0.2227	0.1717

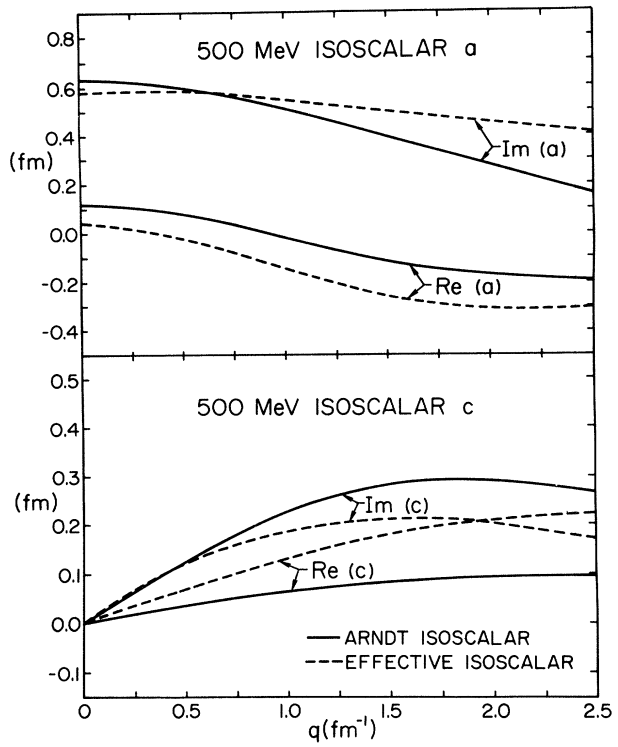

FIG. 5. Components of the 500 MeV isoscalar pN interaction: interaction 2 (dashed curves); IA (free) values from Ref. 13 (solid curves).

part of the Schrödinger-equivalent optical potential out to a momentum transfer of about 2.5 fm^{-1}. Tabulations of the real and imaginary parts of $a(q)$ and $c(q)$ are given in Table I.

Using the effective amplitudes deduced for ^{40}Ca, calculations were carried out for 500 MeV p+$^{40,48}Ca$, ^{90}Zr, and ^{208}Pb elastic scattering using target form factors of the type discussed above. The matter densities for ^{48}Ca, ^{90}Zr, and ^{208}Pb were obtained by the same prescription as for ^{40}Ca. The coefficients of the density squared terms for each nucleus were adjusted according to the prescription

$$z_2=\frac{N_2}{N_1}z_1\frac{\tilde{\rho}^2_{m(1)}(0)}{\tilde{\rho}^2_{m(2)}(0)}, \tag{6}$$

where the subscripts 1 and 2 refer to the reference nucleus (^{40}Ca) and the nucleus of interest, respectively, and N_i is the number of nucleons in nucleus i. Equation (6) ensures that the interaction volume per nucleon remains constant. In Figs. 1–3 are shown (solid curves) the empirical fits to the p+^{40}Ca elastic scattering data,[2,8] along with data and predictions for the p+^{48}Ca, ^{90}Zr, and ^{208}Pb observables.[2,9] As can be seen in the figures, good descriptions of the 500 MeV elastic scattering data are obtained. In appraising this interaction model the success with which the ^{48}Ca, ^{90}Zr, and ^{208}Pb observables are described is noteworthy.

B. Density dependent model

Unfortunately, the form of the optical potential (i.e., the dependence on the density squared form factor) makes the interaction deduced above inconvenient for use in many existing computer codes which calculate proton elastic and inelastic scattering observables. In an effort to find a more applicable form for the optical potential, an alternate density-dependent model was investigated. The central part of the optical potential, Eq. (3), may be written in coordinate space [using the target form factor of Eq. (5)] as

$$U^c_{\rm opt}(\vec{r})=2\pi^2\lambda\int d^3r'\tilde{a}(\vec{r}-\vec{r}')[1+z_i\rho_m(\vec{r}')]\rho_m(\vec{r}'), \tag{7}$$

where

$$\tilde{a}(\vec{r})=\frac{1}{(2\pi)^3}\int d^3q\, e^{i\vec{q}\cdot\vec{r}}a(\vec{q}).$$

Since $\tilde{a}(\vec{r})$ is of short range compared to the nuclear density, it should be a reasonable approximation to write

$$U^c_{\rm opt}(\vec{r})\simeq 2\pi^2\lambda\int d^3r'\tilde{a}(\vec{r}-\vec{r}')[1+z_i\rho_m(\vec{r})]\rho_m(\vec{r}'). \tag{8}$$

One may then redefine the effective spin-independent amplitudes such that they contain explicit density dependence,

TABLE III. Comparison of deduced and theoretical values for $\Delta r_{\rm np}$ and $\Delta r_{\rm nn'}$. All radii are in fm.

Method	^{40}Ca	$\Delta r_{\rm np}$ ^{48}Ca	^{90}Zr	^{208}Pb
This analysis (using effective amplitudes)[a]		0.19	0.05	0.13
Impulse approximation	−0.32	−0.11	−0.25	−0.02
DME	−0.05	0.19	0.08	0.20
HFB	−0.05	0.13	0.06	0.13
	$\Delta r_{\rm nn'}$	(^{48}Ca-^{40}Ca)		
This analysis	0.25			
Impulse approximation	0.22			
DME	0.26			
HFB	0.20			

[a]Errors relative to the ^{40}Ca calculation used to determine the isoscalar amplitudes are estimated to be $\simeq\pm0.04$ fm.

$$a_i^{\text{eff}}(q,r)=a(q)[1+z_i\rho_m(r)] \ . \quad (9)$$

In this form the spin-independent potential is constructed by folding the density dependent interaction with the normal matter density.

Neglecting the small density-squared contributions to the spin-orbit potential (see Table I) and assuming the coefficients, z_i, from Table I for the spin-independent parts, a ^{40}Ca optical potential was generated according to Eq. (8). In Fig. 4 the results for the ^{40}Ca spin observables are compared with the density-squared phenomenological fits from Figs. 2 and 3 and with the data.[2,8] The differential cross section predicted by the density-dependent interaction is equivalent to the fit obtained with the density-squared form shown in Fig. 1. As seen in Fig. 4, this alternate density-dependent form of the effective interaction also provides substantial improvement over IA predictions,[2] although deviations from the trends of the data are noted at larger momentum transfers. Nevertheless, the density-dependent interaction adequately describes the data at small momentum transfers, $\lesssim 2$ fm^{-1}, and should be useful in elastic and inelastic scattering calculations in this momentum transfer range.

III. INTERACTION 2, THE $t\rho$ MODEL

In the preceding section it was demonstrated that good fits to the 500 MeV pA elastic scattering data are obtainable with nonrelativistic optical potentials which are derived from Dirac phenomenology. A prominent feature of these interactions is the density-squared dependence. Such a dependence occurs in Schrödinger-equivalent potentials when one includes intermediate scatterings through negative energy states of the projectile, a purely relativistic effect, in a nonrelativistic equation of motion. What remains to be examined is to what extent the nonrelativistic pA elastic phenomenology *demands* the presence of such density squared terms.

To investigate this issue, an attempt was made to fit the 500 MeV p+^{40}Ca elastic data[2,8] in which the target form factor, $\tilde{F}_{c,\text{so}}(q)$, was constrained to be given by the assumed ^{40}Ca matter density. Since the coefficients, z_i, for the imaginary central and spin-orbit potentials are fairly small (see Table I), the corresponding Im $a(q)$ and $c(q)$ of Table I provided reasonable starting values for use in the fitting procedure. Freely adjusting $a(q)$ and $c(q)$ in Eq. (3) [where only modest changes in Im $a(q)$ and $c(q)$ from the values given in Table I are required] produced the fits (dashed curves) to the ^{40}Ca elastic observables shown in Figs. 1–3. The resulting predictions for p+^{48}Ca, ^{90}Zr, and ^{208}Pb are also shown. In these calculations the small isovector part of the optical potential was included and evaluated using the IA values[13] for the NN isovector interaction. The agreement with the ^{40}Ca data is comparable to that obtained with the density-squared optical model at forward angles, $\lesssim 20°$ c.m. The $t\rho$ potential is, however, somewhat inferior to the density-squared form for large angle scattering, $\gtrsim 20°$–$25°$ c.m. Even so, this $t\rho$ optical potential leads to better agreement with the data[2,8,9] than that obtained using the nonrelativistic impulse approximation. Therefore, from a phenomenological standpoint, the need for large density-squared terms or sizable density dependence in the 500 MeV effective interaction exists at a modest level only. The pA physics underlying the effective interaction models for $a(q)$ and $c(q)$ and the possible density squared terms in the pA optical potential remains to be sorted out.

The components of the 500 MeV effective isoscalar interaction are given in Table II and are compared with the corresponding IA (free) isoscalar amplitudes[13] in Fig. 5. The trends seen in the spin-independent parts of the amplitudes relative to the IA values, such as an overall suppression of Re(a) and a suppression of Im(a) at small q with a decrease in overall slope, are similar to trends observed in G-matrix calculations[4,14] for effective interactions at 300 and 400 MeV when compared with the corresponding IA interaction.[13] On the other hand, the trends of the spin-dependent effective amplitudes relative to the IA interaction appear to be quite different from those observed for G-matrix calculations at lower energies. For example, the deduced Im(c) exhibits a suppression relative to the IA amplitude; G-matrix calculations at 300 and 400 MeV yield substantial enhancements of the effective Im(c) relative to the IA amplitude. The deduced Re(c) shows an enhancement relative to the IA amplitude which is of much greater magnitude than that seen in the lower energy G-matrix results. These differences may suggest the need for including relativistic effects, which are not accounted for in existing G-matrix calculations.

Finally, it is worthwhile to examine the nuclear structure information deduced from fits to the 500 MeV pA elastic scattering data using the $t\rho$ potentials. Calculations were made for p+^{48}Ca, ^{90}Zr, and ^{208}Pb in which the neutron distributions were varied to obtain the best fit to the differential cross section data. These empirical densities were constructed by adding a difference of two Woods-Saxon forms to the neutron densities prescribed in Eq. (4). One of these Woods-Saxon shapes was fixed to approximate the surface geometry of the modified HF density [i.e., the $\rho_n(r)$ computed in Eq. (4)], while the other was adjusted to optimize the fit to the differential cross section data. Such a model for the empirical neutron density permits adjustments to be made to the surface geometry without unduly affecting the nuclear interior. Quantities such as the neutron-proton root-mean-square (rms) radius difference, Δr_{np}, and the isotopic neutron rms radius difference, $\Delta r_{\text{nn}'}$, were obtained. The results are given in Table III where they are compared with IA values[2] and theoretical values from density-matrix-expansion (DME) calculations of Negele[15] and Hartree-Fock-Bogoliubov (HFB) calculations of Gogny.[12] Reasonable agreement is found between quantities deduced using the $t\rho$ potential and theoretical expectations. On the other hand, large discrepancies are noted between theoretical values of Δr_{np} and those deduced from IA fits. Values for $\Delta r_{\text{nn}'}$ exhibit much less variation between effective interaction, IA, and theoretical determinations, suggesting that systematic errors tend to cancel in deduced relative nuclear structure information. Such relative quantities may thus be considered to be accurately determined, but a

more fundamental understanding of the differences between the effective and IA interactions is necessary before deduced *absolute* nuclear structure information, such as Δr_{np} and the neutron density distribution, can be regarded as realistic.

IV. LIMITATIONS ON THE USE OF THE EFFECTIVE INTERACTIONS

The different forms of the optical potentials and effective amplitudes which we have obtained should be useful for a variety of pA elastic and inelastic scattering calculations at and near 500 MeV. However, since only the isoscalar part of the spin-independent and spin-orbit effective interactions were investigated, the results of this study are not applicable to reaction analyses in which isovector and/or tensor pieces of the interaction are important.

The determination of effective amplitudes was limited to momentum transfers of $q \leq 2.5$ fm^{-1} since the existing elastic scattering data are not sensitive to the scattering amplitudes at larger momentum transfers. Reactions which peak at momentum transfers $q \geq 2.0$–2.5 fm^{-1} will be sensitive to larger momentum transfer components of the effective interaction than were investigated here, so that the present interactions are not suitable for such studies. Furthermore, the density dependent form of interaction 1 and the $t\rho$ interaction 2 yield pA observables which deviate from the data as q increases, so that special care should be exercised when using these forms of the effective interaction. However, all of the effective interaction models produce adequate descriptions of the pA elastic scattering observables at small to moderate momentum transfers ($q \leq 2.0$ fm^{-1}) and should be useful for elastic scattering analyses, generation of proton distorted waves, and investigations of inelastic transitions to low-lying natural parity collective states within the above limitations.

V. SUMMARY AND CONCLUSIONS

We have deduced phenomenological isoscalar effective interactions which lead to good descriptions of the 500 MeV pA elastic scattering observables when used within the framework of a nonrelativistic folding model. Effective amplitudes which were derived from the Schrödinger-equivalent Dirac optical potentials provide excellent descriptions of the data at all momentum transfers studied ($q \leq 2.5$ fm^{-1}) when used with a target form factor which is dependent on both the density and the density squared. An alternate density dependent form for the effective interaction also led to a good description of the forward angle ^{40}Ca data.

A $t\rho$ form for the phenomenological optical potential was also assumed and effective amplitudes were obtained, guided by the form of the imaginary spin-independent and spin-orbit parts found for interaction 1. These effective amplitudes also led to good descriptions of the forward angle pA data and reasonable ground state nuclear structure information in the form of Δr_{np} and $\Delta r_{nn'}$.

Our conclusions are the following: (1) Only weak empirical evidence exists for the occurrence of large, density-squared terms in the 500 MeV pA nonrelativistic optical potential; (2) the medium modifications to the IA interaction calculated in Ref. 14 at slightly lower energies seem to reproduce the trends of the empirical spin-independent $t\rho$ interaction but *not* those of the spin-orbit term; (3) the effective interactions presented here are suitable for use in other 500 MeV elastic and inelastic scattering analyses for natural parity, collective excitations when $q \leq 2$ fm^{-1}; and (4) a microscopic understanding of the pA optical potential in this energy range must incorporate medium and relativistic effects, at least, in order to be successful.

This work was supported by the U. S. Department of Energy and The Robert A. Welch Foundation.

[1]A. K. Kerman, H. McManus, and R. M. Thaler, Ann. Phys. (N.Y.) 8, 551 (1959).
[2]G. W. Hoffmann *et al.*, Phys. Rev. Lett. 47, 1436 (1981).
[3]G. W. Hoffmann *et al.*, Phys. Rev. C 24, 541 (1981).
[4]L. Ray, in *The Interactions Between Medium Energy Nucleons in Nuclei—1982,* Proceedings of the Workshop on the Interaction Between Medium Energy Nucleons in Nuclei, Indiana University Cyclotron Facility, 1982, AIP Conf. Proc. No. 97, edited by H. O. Meyer (AIP, New York, 1983), p. 121.
[5]B. C. Clark, S. Hama, R. L. Mercer, L. Ray, and B. D. Serot, Phys. Rev. Lett. 50, 1644 (1983); B. C. Clark *et al.*, Phys. Rev. C 28, 1421 (1983).
[6]J. A. McNeil, J. Shepard, and S. J. Wallace, Phys. Rev. Lett. 50, 1439 (1983); J. Shepard, J. A. McNeil, and S. J. Wallace, *ibid.* 50, 1443 (1983).
[7]L. Ray, Phys. Rev. C 19, 1855 (1979).
[8]A. Rahbar *et al.*, Phys. Rev. Lett. 47, 1811 (1981).
[9]B. Aas *et al.*, Bull. Am. Phys. Soc. 26, 1125 (1981); B. Aas (private communication).
[10]B. C. Clark, S. Hama, and R. L. Mercer, see Ref. 4, p. 260.
[11]I. Sick *et al.*, Phys. Lett. 88B, 245 (1979); J. B. Bellicard *et al.*, Phys. Rev. Lett. 19, 527 (1967); L. A. Fajardo, J. R. Ficenec, W. P. Trower, and I. Sick, Phys. Lett. 37B, 363 (1971); B. Frois *et al.*, Phys. Rev. Lett. 38, 152 (1977).
[12]J. Dechargé and D. Gogny, Phys. Rev. C 21, 1568 (1980); J. Dechargé, M. Girod, D. Gogny, and B. Grammaticos, Nucl. Phys. A358, 203c (1981); J. Dechargé (private communication).
[13]R. A. Arndt *et al.*, Phys. Rev. D 28, 97 (1983); R. A. Arndt (private communication).
[14]H. V. von Geramb, see Ref. 4, p. 44; K. Nakano and H. V. von Geramb (private communication).
[15]J. W. Negele and D. Vautherin, Phys. Rev. C 5, 1472 (1972); the numerical results given here are from the density-matrix-expansion (DME) code of Negele.